Preparation of Nano Spherical α-Fe₂O₃ Supported on 12-Tungstosilicic Acid Using Two Different Methods: A Novel Catalyst

Saghi, Majid; Mahanpoor, Kazem*⁺; Shafiei, Hadi

Department of Chemistry, Arak Branch, Islamic Azad University, Arak, I.R. IRAN

ABSTRACT: *In this research, spherical α-Fe₂O₃ nanoparticles (NPs) were supported on the surface of 12-tungstosilicic acid (12-TSA.7H₂O) as a catalyst support, using two different Forced Hydrolysis and Reflux Condensation (FHRC) and Solid-State Dispersion (SSD) methods. α-Fe₂O₃ and 12-TSA.7H₂O were synthesized due to previous reports. All products were characterized by using FT-IR, SEM, EDX, elemental map, XRD and BET surface area. The results indicated that the supported catalyst (α-Fe₂O₃/12-TSA.7H₂O) successfully was prepared and no change was found on the chemical structures of 12-TSA.7H₂O and α-Fe₂O₃. By using XRD analysis average sizes of spherical α-Fe₂O₃ NPs supported by SSD and FHRC methods were measured 50.5 and 70.82 nm, respectively. The catalyst presented in this study can be applied in the different areas such as nano photocatalytic reactions.*

KEYWORDS: *FHRC; SSD; α-Fe₂O₃; 12-tungstosilicic acid; α-Keggin.*

INTRODUCTION

After remarkable scientific investigations during recent years about nanomaterials, dispersion of NPs on the surface of various organic, inorganic and organic-inorganic catalyst supports was considered significant. Supported NPs play a vital role in heterogeneous catalysis reactions [1]. Metal oxide NPs i.e., iron oxides, have an important position in the science and technologies based on having vast applications and unique properties [2]. α-Fe₂O₃ (hematite) which is the most common forms of iron oxide, has a rhombohedral structure and it is an attractive compound due to its applications in data storage, gas sensor, magnets materials, pigment, catalysis and photocatalysis [3-8].

Various techniques consisting of co-precipitation, sol-gel, thermal decomposition, Micelle synthesis, sonochemical synthesis, hydrothermal synthesis and FHRC have been used to synthesize monodisperse α-Fe₂O₃ NPs [9-15]. So far, distinctive methods have been applied for supporting α-Fe₂O₃ NPs on the surface of the catalyst support. Using these methods depends on the chemical and physical properties of active metal and catalyst support as well as the purpose of the catalytic reaction. One of these methods is FHRC that catalyst support is added to the precursor solution(s), during catalyst preparation (if it was stable in the reaction medium). Besides, the active metal is dispersed on the surface of catalyst support while

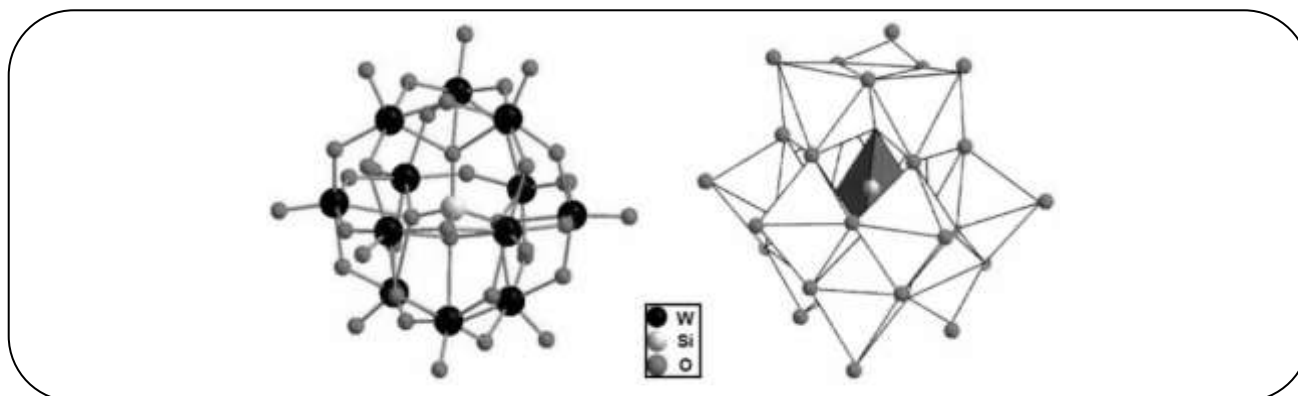*Fig. 1: α-Keggin structure of $[SiW_{12}O_{40}]^{4-}$.*

it is parallel formed. In this method, all steps are related to the synthesis of NPs were done on the catalyst support and final product was obtained after nucleation and growth of NPs. On the other hand, in the SSD method, catalyst precursor and catalyst support are separately synthesized and then are mixed with specific weight percentage ratios, using an appropriate solvent [16]. In addition, during the calcination step, the catalyst is both formed and thermally coated on the surface of catalyst support [17].

Polyoxometalates (POMs) are a great class of inorganic compounds as multi-core metal-oxygen clusters [18]. If a chemical element named heteroatom (such as Si, P, As, B, etc.) enters the molecular structure of POM despite metal and oxygen, then heteropoly acids (HPAs) will be synthesized [19]. In a thermodynamic aspect, HPAs have stable arrangements and maintain their crystal structure in aqueous and non-aqueous solutions. This type of materials have various applications in catalysts [20], photocatalysts [21], analytical chemistry [22], medicinal chemistry (anti-tumor, anti-cancer, anti-bacterial, anti-microbial and anti-clotting) [23-25], radioactive materials [26] and gases absorbent [27] owing to their structural diversity and unique properties. HPAs have different crystal structures from α-, β-, γ-, δ- and ε-Keggin, Wells–Dawson, Preysler, Stromberg, and Anderson–Evans, are served as critical types. 12-tungstosilicic acid (hereafter, 12-TSA) is an HPA with formula $H_4SiW_{12}O_{40}$ and α-Keggin crystal structure (see Fig. 1). The central Si heteroatom is surrounded by a tetrahedron which oxygen vertices are linked to one of the four W_3O_{13} sets. Each W_3O_{13} set consists of three W_3O_6 octahedrals connected in a triangular arrangement by sharing edges and the four W_3O_{13} are linked together by sharing corners [28]. So far, numerous experimental studies have been accomplished about supporting HPAs on the surface of various organic and inorganic catalyst supports, however, HPAs have rarely been used as a catalyst support [29-32].

12-TSA has proper physical and chemical properties in order to be used as a catalyst support. The pores existed on the crystalline surface of 12-TSA provide a suitable condition to support NPs [33]. The high thermal, physical and hydraulic resistance, great crystalline size (6-25 Å), high ion mass, good oxidative potential, reducibility in the presence of light and high acid strength, are chemical specifications of 12-TSA [28,30,33].

Various crystal structures of $α\text{-}Fe_2O_3$ NPs including rod-shape [15], spherical and elliptical forms [34] were synthesized until now. In this research, spherical $α\text{-}Fe_2O_3$ NPs are supported on the surface of 12-TSA.7H_2O through two different SSD and FHRC methods so that a novel catalyst of $α\text{-}Fe_2O_3$/12-TSA.7H_2O could be prepared for the first time. All the synthesized samples were characterized.

EXPERIMENTAL SECTION
Material and apparatuses
All chemicals were used in this study including sodium tungstate dehydrate, sodium silicate, diethyl ether, iron (III) chloride hexahydrate, urea, hydrochloric acid (37% pure) and ethanol purchased from Merck and used without any purification. Also, deionized water was used throughout the experiments. The Fourier Transform Infra-Red (FT-IR) spectra of products were recorded

on a Perkin-Elmer spectrophotometer (Spectrum Two, model) in the range of 450-4000 cm⁻¹. The shape, size, surface morphology and Energy Dispersive X-ray (EDX) spectroscopy of the synthesized 12-TSA.7H₂O and α-Fe₂O₃/12-TSA.7H₂O were characterized using obtained images of a Philips XL-30 Scanning Electron Microscope (SEM). The X-Ray Diffraction (XRD) analysis of the samples was done using a DX27-mini diffractometer and Brunauer, Emmett and Teller (BET) surface area of materials was measured by N_2 adsorption-desorption method at 77 K using a BELSORP-mini II instrument. The samples were degassed under vacuum at 473 K for 12 h before the BET measurement

Synthesis of α-Fe₂O₃ NPs

The synthesis of α-Fe₂O₃ NPs was carried out according to *Bharathi et al.* [15]. Firstly, 100 mL of iron (III) chloride hexahydrate 0.25 M which was considered as a source of Fe^{3+}, was poured into a flat-bottom flask. When Iron solution was agitated by a stirrer, it was added drop by drop to it 100 ml urea 1 M (as a supplying agent of hydroxyl ions). The more gentle and regular adding urea, the smaller and more uniform-sized formed α-Fe₂O₃ particles will be. The obtained mixture was stirred for 30 min and then placed under the reflux at 90-95 ℃ for 12 h. Then, the precipitate after separation was washed with 100 mL deionized water because unreacted ions will be completely removed. The washed precipitate was dried at 70 ℃ for 2 h. Having fully dried, one light brown solid (Iron hydroxide) was yielded. Finally, this solid remained at 300 ℃ for 1 h, hence the iron hydroxide particles will transform to iron oxide. Consequently, a dark brown solid of α-Fe₂O₃ was obtained.

Synthesis of 12-TSA.7H₂O

12-TSA.7H₂O was synthesized according to literature procedure [35]. Firstly, 15 g of sodium tungstate dihydrate was dissolved in 30 ml of deionized water and then 1.16 g sodium silicate solution (density 1.375 g/mL) was added to it. The resulted mixture was heated up to about boiling point, and while it was stirred, 10 mL concentrated HCl was added to it during 30 min, smoothly. Then, the solution was naturally cooled down to RT and the slight precipitate formed (silicic acid) in it was filtered. Again, 5 mL concentrated HCl was added to the solution and was transferred to separatory funnel after cooling it again

down to RT. Then, 12mL of diethyl ether was added to it and well shaken. Therefore, three layers were formed inside the separatory funnel, a middle layer of which was yellow-colored. Bottom layer which was oily ether was separated and transferred to a beaker. In order to further extract, the separatory funnel was further shaken again and the bottom layer was once more separated and transferred into the beaker. This extraction process was done so much that the yellow color of the middle layer was fully faded. The extracted ether complex which was inside the beaker was transferred to another separatory funnel and then 16 ml HCl 25% (v/v) was added to it. Next, 4 mL diethyl ether was added to it, subsequently. The contents inside separatory funnel were shaken and the bottom layer (ether) was transferred to the evaporating dish after separating. The evaporating dish was exposed to air and remained motionless to evaporate the solvent and form the 12-TSA.7H₂O crystals. Finally, 12-TSA.7H₂O formed crystals were placed at 70 ℃ for 2 h until it was completely dried. The chemical reaction occurred in the process of 12-TSA.7H₂O synthesis has been shown in Equation (1) [35].

$$12Na_2WO_4 + NaSiO_3 + 26HCl \rightleftarrows \qquad (1)$$
$$H_4SiWl_2O_{40} \cdot xH_2O + 26NaCl + 11H_2O$$
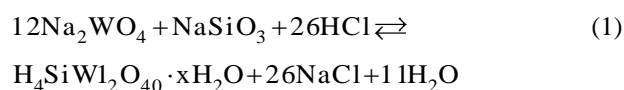
Preparation of α-Fe₂O₃/12-TSA.7H₂O
FHRC method

Scheme 1 shows a flowchart of the experimental procedure used to synthesis α-Fe₂O₃/12-TSA.7H₂O through FHRC method. Firstly, 50 mL of iron (III) chloride hexahydrate 0.25 M was poured into a beaker. While it was agitated by a stirrer, 3.5 g 12-TSA.7H₂O was gently added to it. The obtained mixture was stirred for 4-5 h. Then, stirring was stopped for 2 h until the solid within the mixture was deposited. The solid accumulated at bottom of the beaker was separated and transferred into one flat-bottom flask and the same 10 mL solution inside beaker was added to it. When mixture inside flat-bottom flask was being stirred, 50 ml urea 1 M was gradually added to it. The mixture was placed under reflux at 90-95 ℃ for 12 h. Then, the precipitate resulted after separation was washed with 100 ml ethanol/deionized water 1:1 solution because unreacted ions were completely removed. The washed precipitate was dried in the air for 2 h and then was kept at 80 ℃ for 2 h. In order to calcination, the obtained solid was kept at 300 ℃ for 1 h.
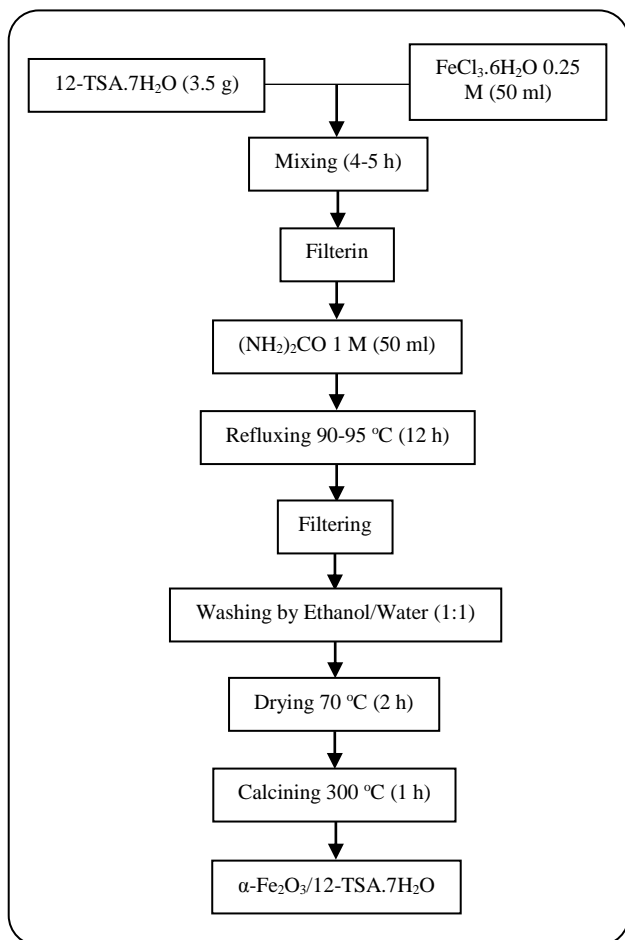
Scheme 1: Flowchart of the preparation of α-Fe₂O₃/12-TSA.7H₂O via FHRC method.
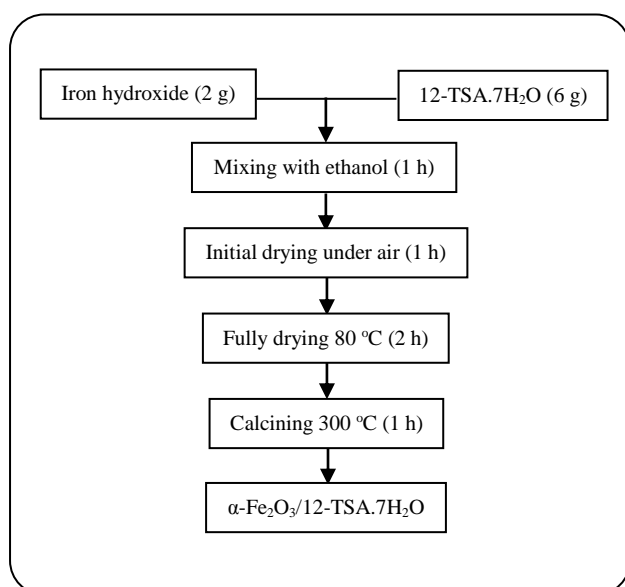
Scheme 2: Simplified flowsheet of α-Fe₂O₃/12-TSA.7H₂O preparation process through the SSD method.

SSD method

Scheme 2 shows a simplified flowsheet for $\alpha\text{-}Fe_2O_3$/12-TSA.7H₂O preparation process through SSD method. Firstly, the synthesized iron hydroxide (light brown solid) and 12-TSA.7H₂O catalyst support were mixed with a weight ratio of 1:3 iron hydroxide/12-TSA.7H₂O (weight of catalyst support is three times of catalyst weight) using an agate pestle and mortar for 1 h. In order to have a better mixture, ethanol was sprayed on the mixture until it becomes dough-form. During mixing, in the vaporization phase, ethanol is again added in order to keep the dough-form of the mixture. The resulted mixture was dried under air for 1 h and then was kept at 80 ºC for 2 h. In order to do calcination and transform iron hydroxide particles fixed on the surface of 12-TSA.7H₂O into iron oxide ($\alpha\text{-}Fe_2O_3$), the obtained solid was kept at 300 ºC for 1 h.

RESULTS AND DISCUSSION

Characterization

The synthesized 12-TSA.7H₂O

SEM image of the synthesized 12-TSA.7H₂O was shown in Fig. 2. Surface morphology of 12-TSA.7H₂O shows that this sample has a proper structural property and can be considered as a catalyst support. In other words, the pores which are on the surface of this catalyst support provide a breeding ground to support $\alpha\text{-}Fe_2O_3$ NPs. IR is a suitable method for the structural characterization of HPAs [19]. FT-IR spectrum of the synthesized 12-TSA.7H₂O was shown in Fig. 3. There are four kinds of oxygen atoms in 12-TSA.7H₂O structure. 4 Si-O_a in which one oxygen atom connects to Si, 12 W-O_b-W oxygen bridges (corner-sharing oxygen-bridge between different W_3O_{13} groups), 12 W-O_c-W oxygen bridges (edge-sharing oxygen-bridge within W_3O_{13} groups) and 12 W=O_d terminal oxygen atoms. The symmetric and asymmetric stretching of the different kinds of W-O bonds were observed in the following spectral regions: Si-O_a bonds (1020 cm^{-1}), W=O_d bonds (1000-960 cm^{-1}), W-O_b-W bridges (890-850 cm^{-1}), W-O_c-W bridges (800-760 cm^{-1}) [36]. In Table 1, the vibrational frequencies of the synthesized 12-TSA.7H₂O and equivalent values which were reported in former studies [36, 37] have been listed. Comparing the vibrational frequencies between samples reveals that, 12-TSA.7H₂O was synthesized properly. Fig. 4 shows the XRD pattern
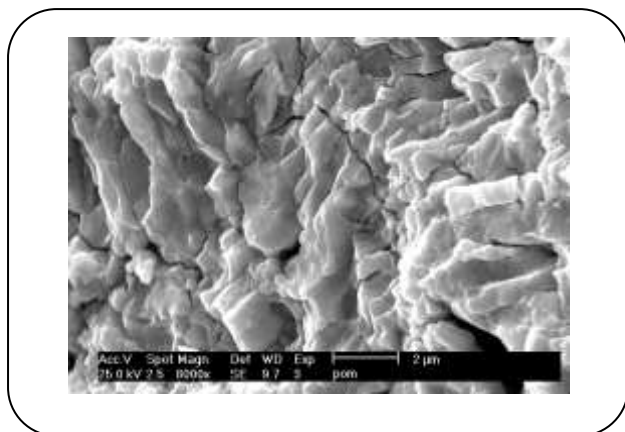
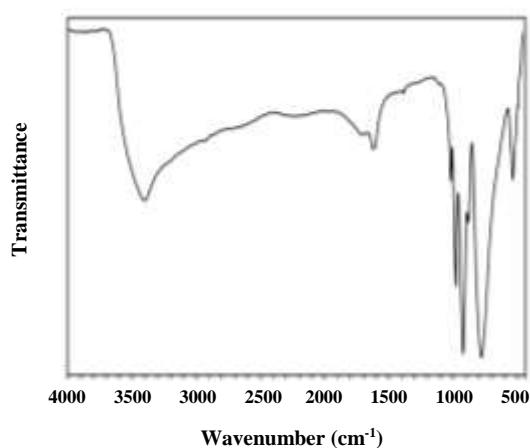**Fig. 2: SEM image of the synthesized 12-TSA.7H₂O.**

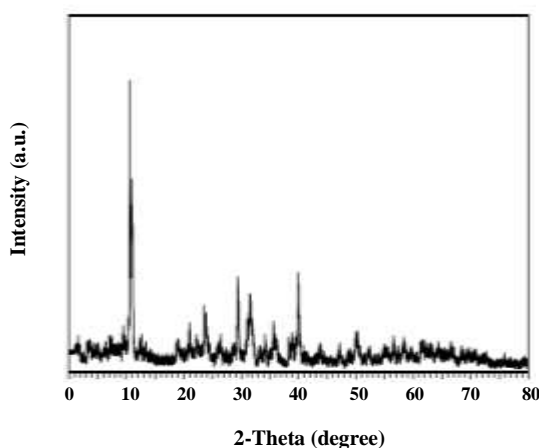**Fig. 3: FT-IR spectrum of the synthesized 12-TSA.7H₂O.**

Fig. 4: XRD pattern of the synthesized 12-TSA.7H₂O.

of the synthesized 12-TSA.7H₂O. This pattern indicates that the characteristic peaks corresponded to the 12-TSA, were appeared clearly and it means that 12-TSA.7H₂O crystals were formed properly [37]. The BET surface area of 12-TSA.7H₂O was 11.76 (m^2/g).
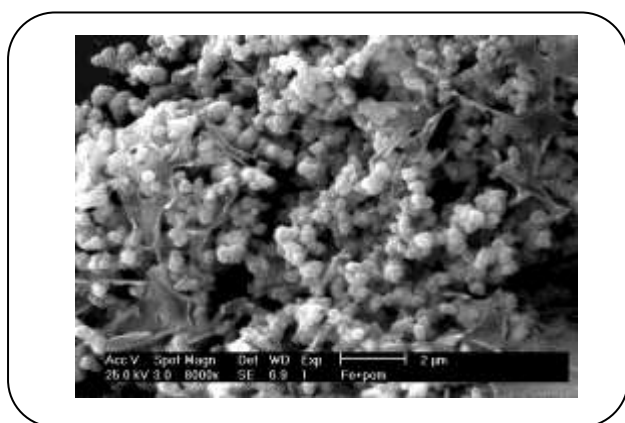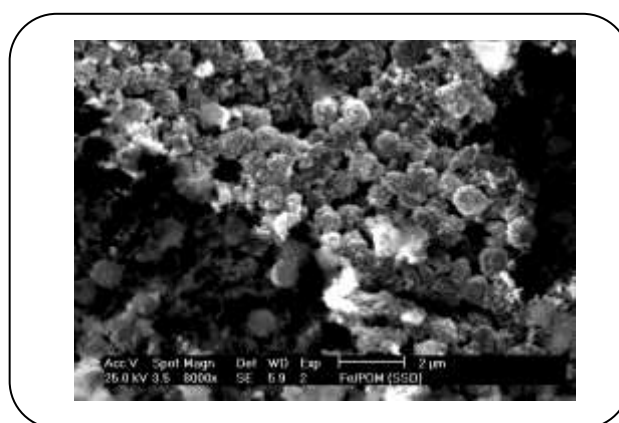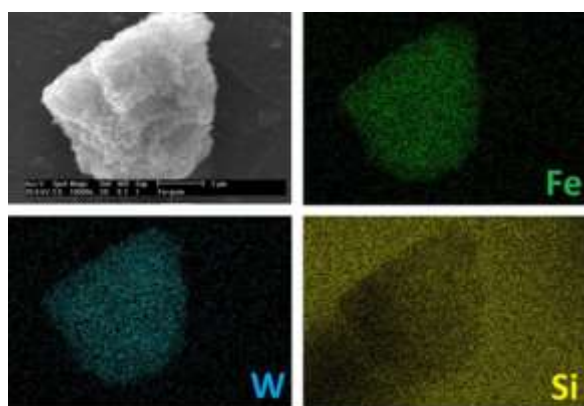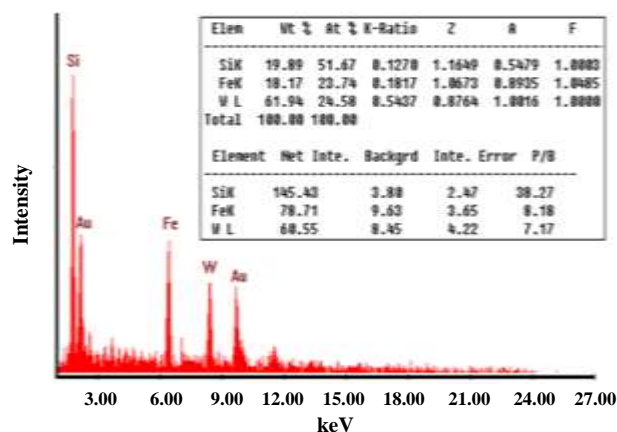
The prepared α-Fe₂O₃/12-TSA.7H₂O

Figs. 5 and 6 show the SEM image of α-Fe₂O₃/12-TSA.7H₂O were prepared by FHRC and SSD methods, respectively. These images indicate that in both methods, α-Fe₂O₃ NPs were spherically supported on the surface of 12-TSA.7H₂O. The formed spheres in the SSD method are larger and have coated more area of 12-TSA.7H₂O than FHRC method. Probably in the SSD method, spherical α-Fe₂O₃ particles adhered to each other and have formed larger spheres, however, it did not occur in FHRC method that is α-Fe₂O₃ particles were separately supported. Possible reasons are as follows: Firstly, probably, α-Fe₂O₃ synthesized particles by SSD method are smaller than the FHRC method and this contributed to their adherence. Secondly, supporting through SSD method was done in solid state and this increases the possibility of particles adhering to each other and forming larger spheres. Finally, supporting through FHRC method was done in the liquid phase, so the particles could freely convey and be separately fixed on the 12-TSA.7H₂O surface.

EDX is an analytical technique, which is used for the elemental analyses or chemical characterization. This technique, which has the capability of quantitative and qualitative analysis, could be effective in measuring the number of elements existed in the sample. In order to consider iron particles distribution on the 12-TSA.7H₂O surface and analyze other elements, elemental maps of α-Fe₂O₃/12-TSA.7H₂O were captured. Figs. 7 and 8, displays the EDX spectrum and element map of α-Fe₂O₃/12-TSA.7H₂O prepared by FHRC and SSD methods, respectively. It is necessary to note that the emergence of Au peaks is due to samples coverage's with a thin layer of gold before SEM/EDX analysis. In EDX spectra, peaks of three main elements in α-Fe₂O₃/12-TSA.7H₂O namely Si, W, and Fe were detected and named. Si and W are related to the 12-TSA.7H₂O catalyst support and Fe is related to the α-Fe₂O₃ NPs. As it is seen, Si and W peaks which are related to 12-TSA.7H₂O, which have more intensity in the EDX spectrum of α-Fe₂O₃/12-TSA.7H₂O prepared by FHRC compare to equivalent peaks

Table 1: Vibrational frequencies of the synthesized 12-TSA.7H₂O and equivalent values reported in previous reports.

Number	The synthesized 12-TSA.7H₂O		[36,37]
	Wavenumber (cm⁻¹)	Transmittance %	
1	1019.04	13.29	1020 (weak)
2	980.68	8.81	981 (sharp)
3	924.31	5.92	928 (very sharp)
4	882.63	11.52	880 (medium)
5	780.28	5.77	785 (very sharp)
6	537.41	13.35	540 (medium)

Fig. 5: SEM image of α-Fe₂O₃/12-TSA.7H₂O prepared by the FHRC method.

Fig. 6: SEM image of α-Fe₂O₃/12-TSA.7H₂O prepared by the SSD method.

Fig. 7: EDX spectrum and elemental map of α-Fe₂O₃/12-TSA.7H₂O prepared by FHRC method.

in the EDX spectrum of α-Fe₂O₃/12-TSA.7H₂O prepared by the SSD method. Besides, comparison of EDX spectrums, it was clear that, Fe peak in the EDX spectrum of α-Fe₂O₃/12-TSA.7H₂O which was prepared by SSD has more intensity than the Fe peak in the EDX spectrum of α-Fe₂O₃/12-TSA.7H₂O prepared by FHRC. On the other hand, these support analyzed by SEM characterization and the results show that during supporting step by SSD method, 12-TSA.7H₂O surface was covered by more amount of α-Fe₂O₃ than that of FHRC method. According to
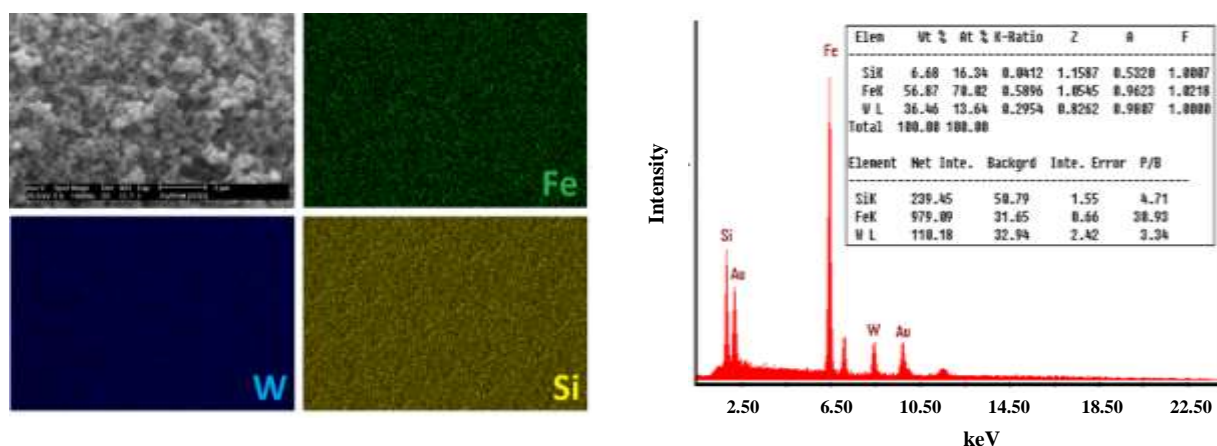
Fig. 8: EDX spectrum and elemental map of α-Fe₂O₃/12-TSA.7H₂O prepared by SSD method.
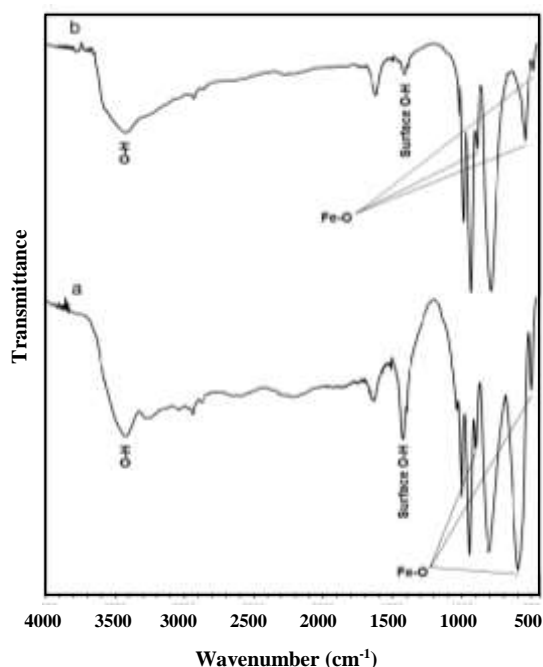

*Fig. 9: FT-IR spectra of α-Fe₂O₃/12-TSA.7H₂O prepared by SSD (a) and FHRC (b) methods.*

the Fe map in Fig. 7, lack of green spots around the particle and uniform distribution of the above particle area, prove that α-Fe₂O₃ NPs were supported properly on the surface of α-Fe₂O₃/12-TSA.7H₂O. One of the substantial points was, based on Si map; yellow spots were found around particle and in particle area too. Because the α-Fe₂O₃/12-TSA.7H₂O solid powder was placed above glass base (in order to analysis) and since glass has been made of silicon, areas close to particle are yellow which is completely normal.

In Fig. 9a and b, FT-IR spectra of α-Fe₂O₃/12-TSA.7H₂O prepared by SSD and FHRC methods, were shown, respectively. It is clear that absorption peaks of 12-TSA.7H₂O appeared without significant change in the wavenumbers (only their intensities were slightly changed). In other words, in both methods, 12-TSA.7H₂O was stable and its chemical structure was not changed, during preparing α-Fe₂O₃/12-TSA.7H₂O catalyst. In addition, absorption peaks of α-Fe₂O₃ were detected clearly and were in agreement with Bharati et al results [15]. These absorption peaks which are related to stretching and bending modes of OH and Fe-O binding in FeOOH, overlapped in some samples with absorption peaks of 12-TSA.7H₂O. Comparing FTIR spectra revealed that absorption peaks of α-Fe₂O₃ related to SSD method were more intense than that of the FHRC method. This pattern almost confirms the results of SEM images. Furthermore, in the SSD method, the surface of 12-TSA.7H₂O was covered by more α-Fe₂O₃ particles.

In Fig. 10a and b, XRD patterns of α-Fe₂O₃/12-TSA.7H₂O prepared by SSD and FHRC methods, illustrated, respectively. In both of these patterns, characteristic peaks of 12-TSA.7H₂O were appeared properly, which indicates that 12-TSA.7H₂O was stable during supporting process in both SSD and FHRC methods. In these patterns, the characteristic peaks of α-Fe₂O₃ which were also marked appeared and it was in agreement with Bharati et al results [15]. In XRD related to SSD method, the intensity of 12-TSA.7H₂O and α-Fe₂O₃ characteristic peaks are lower and higher than the FHRC method, respectively. This trend confirms the results of SEM and FT-IR, hence during supporting through the SSD method,

Table 2: BET surface area of products.

Product	BET surface area (m^2/g)
12-TSA.7H$_2$O	11.76
α-Fe$_2$O$_3$/12-TSA.7H$_2$O prepared by FHRC Method	39.84
α-Fe$_2$O$_3$/12-TSA.7H$_2$O prepared by SSD Method	57.53
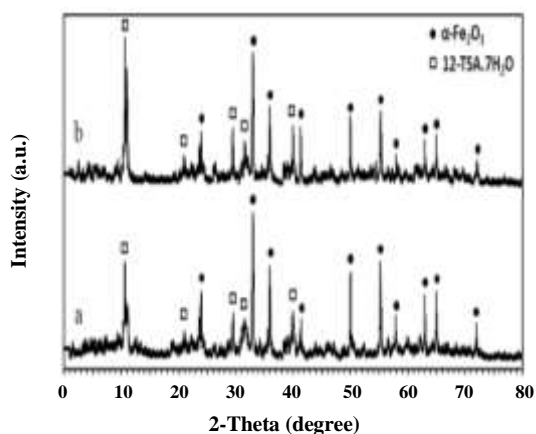
Fig. 10: X-ray diffractogram of α-Fe₂O₃/12-TSA.7H₂O prepared by SSD (a) and FHRC (b) methods.

12-TSA.7H$_2$O surface was covered by the greater amount of α-Fe$_2$O$_3$ particles. The size of the spherical α-Fe$_2$O$_3$ particles was supported on the surface of 12-TSA.7H$_2$O measured by XRD outcome using Warren-Averbach method (taking account of device errors). The average crystal sizes for SSD and FHRC methods were obtained 50.5 and 70.82 nm, respectively.

BET surface area of α-Fe$_2$O$_3$/12-TSA.7H$_2$O prepared through FHRC and SSD methods were reported in Table 2 which measured 39.84 and 57.53 (m^2/g), respectively. Based upon the surface area of α-Fe$_2$O$_3$/12-TSA.7H$_2$O prepared by SSD is larger than α-Fe$_2$O$_3$/12-TSA.7H$_2$O surface area, prepared by the FHRC method, it was concluded that α-Fe$_2$O$_3$/12-TSA.7H$_2$O prepared by SSD probably has more catalytic activity than α-Fe$_2$O$_3$/12-TSA.7H$_2$O catalyst, prepared by the FHRC method due to, catalyst prepared by the SSD method has more accessible active sites than the catalyst prepared by FHRC method for chemical reactions.

CONCLUSIONS

In this study, spherical α-Fe$_2$O$_3$ NPs were successfully supported on the surface of 12-TSA.7H$_2$O by SSD and

FHRC methods which shows the effectiveness of these methods clearly. The results of qualitative and quantitative characterization indicated that:

1- In both methods were used in the study, α-Fe$_2$O$_3$ NPs were spherically synthesized and supported on the surface of 12-TSA.7H$_2$O.

2- In both methods were used, 12-TSA. The 7H$_2$O structure did not change chemically during preparation and could well support the α-Fe$_2$O$_3$ particles due to its stability.

3- The average crystal sizes of α-Fe$_2$O$_3$ particles supported through SSD and FHRC methods are 50.5 nm and 70.82 nm respectively. Therefore NPs supported by SSD method were smaller, which is considered very significant.

4- In the SSD method, 12-TSA.7H$_2$O surface will be covered by much more α-Fe$_2$O$_3$ particles while, in the FHRC method, α-Fe$_2$O$_3$ NPs dispersion on the surface of 12-TSA.7H$_2$O will be more regular and monodisperse.

5- Element maps of synthesized catalysts shown that the particle distributions of iron oxide on the surface of the catalyst support were made uniformly.

6- The novel introduced catalyst in this research could be used in different contexts such as nano photocatalytic reactions.

REFERENCES

[1] George S. M., Introduction: Heterogeneous Catalysis, *Chem. Rev*. **95**(3): 475-476 (1995).

[2] Xia Y., Xiong Y., Lim B., Skrabalak S. E., Shape-Controlled Synthesis of Metal Nanocrystals: Simple Chemistry Meets Complex Physics?, *Angew. Chem. Int. Ed*., **48**(1): 60-103 (2009).

[3] Jun Y. W., Choi J. S., Cheon J., Heterostructured Magnetic Nanoparticles: Their Versatility and High Performance Capabilities, *Chem. Commun*., **12**: 1203-1214 (2007).

[4] Chen J., Xu L., Li W., Gou X., α-Fe$_2$O$_3$ Nanotubes in Gas Sensor and Lithium-ion Battery Applications, *Adv. Mater*., **17**(5): 582-586 (2005).

[5] Raming T. P., Winnubst A. J. A., Van Kats C. M., Philipse A. P., The Synthesis and Magnetic Properties of Nanosized Hematite (α-Fe$_2$O$_3$) Particles, *J. Colloid Interface Sci*., **249**(2): 346-350 (2002).

[6] Walter D., Characterization of Synthetic Hydrous Hematite Pigments, *Thermochim. Acta*., **445**(2): 195-199 (2006).

[7] Shekhah O., Ranke W., Schüle A., Kolios G., Schlögl R., Styrene Synthesis: High Conversion over Unpromoted Iron Oxide Catalysts Under Practical Working Conditions, *Angew. Chem. Int. Ed*., **42**(46): 5760-5763 (2003).

[8] Mishra M., Chun D. M., α-Fe₂O₃ as a Photocatalytic Material: A Review, *Appl. Catal. A*., **498**: 126-141 (2015).

[9] Farahmandjou M., Soflaee F., Synthesis and Characterization of α-Fe₂O₃ Nanoparticles by Simple Co-Precipitation Method, *Phys. Chem. Res*., **3**(3): 191-196 (2015).

[10] Liang H., Liu K., Ni Y., Synthesis of Mesoporous α-Fe₂O₃ via Sol–Gel Methods Using Cellulose Nano-Crystals (CNC) as Template and its Photo-Catalytic Properties, *Mater. Lett*., **159**: 218-220 (2015).

[11] Diab M., Mokari T., Thermal Decomposition Approach for the Formation of α-Fe₂O₃ Mesoporous Photoanodes and an α-Fe₂O₃/CoO Hybrid Structure for Enhanced Water Oxidation, *Inorg. Chem*., **53**(4): 2304-2309 (2014).

[12] Jiang T., Poyraz A. S., Iyer A., Zhang Y., Luo Z., Zhong W., Miao R., El-Sawy A. M., Guild C. J., Sun Y., Kriz D. A., Suib S. L., Synthesis of Mesoporous Iron Oxides by an Inverse Micelle Method and Their Application in the Degradation of Orange II Under Visible Light at Neutral pH, *J. Phys. Chem. C*., **119**(19): 10454-10468 (2015).

[13] Askarinejad A., Bagherzadeh M., Morsali A., Sonochemical Fabrication and Catalytic Properties of α-Fe₂O₃ Nanoparticles, *J. Exp. Nanosci*., **6**(3): 217-225 (2011).

[14] Tadic M., Panjan M., Damnjanovic V., Milosevic I., Magnetic Properties of Hematite (α-Fe₂O₃) Nanoparticles Prepared by Hydrothermal Synthesis Method, *Appl. Surf. Sci*., **320**: 183-187 (2014).

[15] Bharathi S., Nataraj D., Mangalaraj D., Masuda Y., Senthil K., Yong K., Highly Mesoporous α-Fe₂O₃ Nanostructures: Preparation, Characterization and Improved Photocatalytic Performance Towards Rhodamine B (RhB), *J. Phys. D: Appl. Phys*., **43**: 1-9 (2010).

[16] Nikazar M., Gholivand K., Mahanpoor K., Photocatalytic Degradation of Azo Dye Acid Red 114 in Water with TiO₂ Supported on Clinoptililite as a Catalyst, *Desalination*., **219**(1-3): 293-300 (2008).

[17] Dehno Khalaji A., Solid State Process for Preparation of Nickel Oxide Nanoparticles: Characterization and Optical Study, *Iran. J. Chem. Chem. Eng. (IJCCE)*, **35**(3): 17-20 (2016).

[18] Hill C. L., Polyoxometalates, *Chem. Rev*., **98**(1): 1-387 (1998).

[19] Pope M. T., "Heteropoly and Isopoly Oxometalates", Springer-Verlag Berlin Heidelberg, Berline (1983).

[20] Kozhevnikov I. V., Catalysis by Heteropoly Acids and Multicomponent Polyoxometalates in Liquid-Phase Reactions, *Chem. Rev*., **98**(1): 171-198 (2012).

[21] Zhong J. B., Photocatalytic Decolorization of Methyl Orange Solution with Phosphotungstic Acid, *Iran. J. Chem. Chem. Eng. (IJCCE)*, **32**(1): 57-65 (2013).

[22] Es'haghi Z., Hooshmand S., Dispersive Solid-Liquid Phase Microextraction Based on Nanomagnetic Preyssler Heteropolyacid: A Novel Method for the Preconcentration of Nortriptyline, *J. Sep. Sci*., **38**(9): 1610-1617 (2015).

[23] Wang L., Zhou B., Liu J., Anticancer Polyoxometalates, *Prog. Chem.*, **25**(7): 1131-1141 (2013).

[24] Judd D. A., Netlles H. J., Nevis N., Snyder J. P., Liotta D. C., Tang J., Ermolieff J. J., Schinazi F. R., Hill C. L., Polyoxometalate HIV-1 Protease Inhibitors. A New Mode of Proteas Inhibition, *J. Am. Chem. Soc*., **123**(5): 886-897 (2001).

[25] Wang X., Liu J., Li J., Liu J., Synthesis, Characterization and in Vitro Antitumor Activity of Diorganometallo Complexes γ-Keggin Anions, *Inorg. Chem. Commun*., **4**(7): 372-374 (2001).

[26] Lin Z., Zhongqun L., Wenjun C., Shaojin C., Removing Cs from Nuclear Waste Liquid by Crown Ether and Heteropoly Acid: Simulated Tests, *J. Radioanal. Nucl. Chem*., **205**(1): 49-56 (1996).

[27] Heylen S., Smeekens S., Kirschhock C. E. A., Parac-Vogt T. N., Martens J. A., Temperature Swing Adsorption of NOx over Keggin Type Heteropolyacids, *Energy Environ. Sci*., **3**(7): 910-916 (2010).

[28] Lihua B., Qizhuang H., Qiong J., Enbo W., Synthesis, Properties and Crystal Structure of $(Gly)_2H_4SiW_{12}O_{40}.5.5H_2O$, *J. Mol. Struct*., **597**(1-3): 83-91 (2001).

[29] Soled S., Miseo S., McVicker G., Gates W. E., Gutierrez A., Paes J., Preparation and Catalytic Properties of Supported Heteropolyacid Salts, *The Chemical Engineering Journal and the Biochemical Engineering Journal*., **64**(2): 247-254 (1996).

[30] Abolghasemi M. M., Hassani S., Rafiee E., Yousefi V., Nanoscale-Supported Heteropoly Acid as a New Fiber Coating for Solid-Phase Microextraction Coupled with Gas Chromatography-Mass Spectrometry, *J. Chromatogr. A*., **1381**: 48-53 (2015).

[31] Chen F., Ma J., Dong Z., Liu R., Characterization and Catalytic Performance of Heteropoly Acid $H_4SiW_{12}O_{40}$ Supported on Nanoporous Materials, *J. Nanosci. Nanotechnol*., **14**(9): 7293-7299 (2014).

[32] Badday A. S., Abdullah A. Z., Lee K. T., Transesterification of Crude Jatropha Oil by Activated Carbon-Supported Heteropolyacid Catalyst in an Ultrasound-Assisted Reactor System, *Renewable Energy*., **62**: 10-17 (2014).

[33] Taylor D. B., McMonagle J. B., Moffat J. B., Cation Effects on the Surface and Bulk Structure of the Salts of 12-Tungstosilicic Acid, *J. Colloid Interface Sci*., **108**(1): 278-284 (1985).

[34] Jiao H., Wang J., Single Crystal Ellipsoidal and Spherical Particles of α-Fe_2O_3: Hydrothermal Synthesis, Formation Mechanism, and Magnetic Properties, *J. Alloys Compd*., **577**: 402-408 (2013).

[35] North E. O., Bailar J. C., Jonelis F. G., Silicotungstic Acid, *Inorg. Synth*., **1**: 129-132 (2007).

[36] Bamoharram F. F., Vibrational Spectra Study of the Interactions Between Keggin Heteropolyanions and Amino Acids, *Molecules*., **14**(9): 3214-3221 (2009).

[37] Kozhevnikov I. V., Sinnema A., Jansen R. J. J., Bekkum H. V., ^{17}O NMR Determination of Proton Sites in Solid Heteropoly Acid $H_3PW_{12}O_{40}$. ^{31}P, ^{29}Si and ^{17}O NMR, FT-IR and XRD Study of $H_3PW_{12}O_{40}$ and $H_4SiW_{12}O_{40}$ Supported on Carbon, *Catal. Lett*., **27**(1-2): 187-197 (1994).